Research Square

Preprints are preliminary reports that have not undergone peer review.
They should not be considered conclusive, used to inform clinical practice,
or referenced by the media as validated information.

Probing Kaniadakis Holographic Dark Energy in a Bianchi Type-V Self-Creation Universe: Dynamics and Diagnostics

M. P.V.V. BhaskaraRao

Vignan's Institute of Information Technology (A)

Tenneti Ramprasad

ramprasad@staff.vce.ac.in

Vasavi College of Engineering (A)

Research Article

Keywords: Bianchi type-V cosmology, Kaniadakis holographic dark energy, Self-creation theory, Anisotropic dark energy, Hybrid expansion law, Generalized second law

Posted Date: November 20th, 2026

DOI: https://doi.org/10.21203/rs.3.rs-11596513/v1

License: This work is licensed under a Creative Commons Attribution 4.0 International License.
Read Full License

Additional Declarations: No competing interests reported.

Probing Kaniadakis Holographic Dark Energy in a Bianchi Type-V Self-Creation Universe: Dynamics and Diagnostics

M.P.V.V. BhaskaraRao[1] · Tenneti Ramprasad[2*]

[1]Department of Basic Sciences and Humanities, Vignan's Institute of Information Technology (A), Visakhapatnam, Andhra Pradesh, India

[2]Department of Mathematics, Vasavi College of Engineering (A), Hyderabad, Telangana, India

***Corresponding author:** Tenneti Ramprasad, e-mail: ramprasad@staff.vce.ac.in

E-mail of co-author: M.P.V.V. BhaskaraRao, mekabhaskar@vignaniit.edu.in

ORCID: M.P.V.V. BhaskaraRao https://orcid.org/0000-0001-6347-4156; Tenneti Ramprasad https://orcid.org/0000-0002-5599-1118

Abstract

We study a spatially homogeneous and anisotropic Bianchi type-V universe in Barber's second self-creation theory of gravitation, filled with pressureless dark matter and an anisotropic Kaniadakis holographic dark energy (KHDE) fluid with a Hubble-horizon cutoff. We show that the off-diagonal field equation forces the two skewness parameters of the dark-energy fluid to be equal and opposite, $\delta = -\gamma$, so that a fluid with two equal principal pressures is necessarily isotropic. Moreover, the vanishing-trace condition often used to integrate the scalar-field equation is equivalent to a vanishing Ricci scalar and over-determines the system; instead, we integrate the scalar-field equation as a linear equation driven by the Ricci scalar. The field equations are closed by the Collins relation between the metric potentials and a hybrid expansion law. The model describes a smooth transition from deceleration to acceleration (at $t \approx 2.07$ for representative parameters), keeps a positive dark-matter density and has a constant shear-to-expansion ratio set by the Collins exponent. The KHDE equation-of-state parameter evolves from a matter-like value through the quintessence region and crosses the phantom divide (quintom-like behaviour), while the skewness parameters remain of order 0.1. The squared sound speed indicates late-time instability. The statefinder pair approaches the Λ cold dark matter (ΛCDM) point at late times, and the energy conditions, the Om diagnostic and the ω–ω' plane are also analysed. The generalized second law of thermodynamics at the apparent horizon holds for weak scalar coupling but is violated at late times for stronger coupling.

Keywords Bianchi type-V cosmology · Kaniadakis holographic dark energy · Self-creation theory · Anisotropic dark energy · Hybrid expansion law · Generalized second law

1 Introduction

Numerous independent astronomical data, including Type Ia supernovae, the cosmic microwave background, and large-scale structure surveys, support the present acceleration of the Universe's expansion [1–3]. Dark energy (DE), a component with negative pressure whose physical origin is one of the main unresolved issues in modern cosmology, is invoked in the mainstream explanation. The cosmological constant Λ, the most straightforward choice, is in good accord with the evidence but has significant cosmic-coincidence and fine-tuning issues. A wide class of dynamical dark energy models are motivated by these issues. Dark energy and the holographic principle [4,5], which limits a region's entropy by its boundary area rather than its volume, are particularly appealing lines of investigation. Holographic dark energy (HDE) models construct the dark energy density from the entropy–area relation of an infrared cut-off, often the Hubble horizon, in accordance with the vacuum-energy bound of Cohen et al. [6]. The observed equation of state has been successfully replicated by them. The choice of horizon entropy determines the density's functional shape. The initial HDE concept made use of the Bekenstein–Hawking entropy. Subsequent research has employed generalized entropies including Tsallis [7], Rényi [8], Barrow, and Kaniadakis entropy, which result in a distinct holographic density and more complex dynamics. A relativistic one-parameter extension of the Boltzmann–Gibbs statistics, the Kaniadakis entropy [9] eventually reduces to the Bekenstein entropy. The Kaniadakis holographic dark energy (KHDE) [10] is an extension of the thermodynamically justified HDE framework, which is gaining popularity.

Later, the KHDE has been studied in many space-times and modified theories of gravity [11,12]. Prasanthi et al. [13] have studied the cosmic dynamics of a KHDE model in anisotropic Brans–Dicke background. Aditya et al. [14] have reconstructed the KHDE model in self-creation theory. Murali et al. [15] performed a cosmographic analysis of an anisotropic KHDE model. Ganeswara Rao et al. [16] studied a Bianchi type-VI_0 KHDE model in Brans–Dicke gravity. Other generalized entropies have also been used to construct holographic models. Examples are Sharma–Mittal holographic dark energy model of Vijaya Prasanthi et al. [17], modified holographic Ricci dark energy model of Rao and Divya Prasanthi in Bianchi type-V background [18], Bianchi type-VI_0 KHDE model in general relativity of Rao et al. [19] and bulk viscous Bianchi type-II string cosmology in self-creation theory of Reddy et al. [20]. Barber's self-creation theory [21] modifies general relativity by allowing the gravitational coupling to vary through a scalar field, while remaining consistent with solar-system tests.

The Bianchi type-V space-times are a generalization of the open Friedmann–Lemaître–Robertson–Walker geometry to allow for small, spatially homogeneous anisotropies. Thus they provide a natural and analytically tractable setting in which to test whether such anisotropies decay as the Universe evolves. We combine these two frameworks with the Kaniadakis holographic prescription to study the effects of the deformed entropy content and the varying gravitational coupling on the geometry and the late time dynamics of an anisotropic universe. The present work is an extension of recent study of Bianchi type-V universe filled with generalized ghost pilgrim dark energy in the same self-creation framework [22]. We retain the background geometry and the theory of gravity, and replace the dark-energy prescription by the Kaniadakis holographic construction so as to isolate the effect of the dark-energy sector onto the anisotropic dynamics.

Two technical points shape the construction and constitute the main theoretical results of this work. First, we demonstrate in Section 3 that, for the Bianchi type-V metric, the off-diagonal field equation forces the skewness parameters of the dark-energy fluid along the y- and z-directions to be equal and opposite. Therefore, a dark-energy stress tensor with two equal principal pressures is inherently isotropic, and both skewness parameters, δ and γ, are necessary for a fluid to be genuinely anisotropic. This result follows from the field equations alone and holds independently of the dark-energy model adopted here. Second, the vanishing-trace condition, commonly employed to integrate the scalar-field equation in self-creation cosmology [23], is equivalent to a vanishing Ricci scalar; it therefore over-determines the system and is violated by the solution obtained here. We instead solve the scalar-field equation directly, as a linear equation driven by the Ricci scalar. Collins' relation between the metric potentials [24] and a hybrid expansion law for the average scale factor [25], which permits the transition from deceleration to acceleration, are used to close the system.

The paper is structured as follows. The metric and field equations are introduced in Section 2, and the solution is obtained in Section 3. Section 4 discusses kinematical and physical characteristics. Section 5 provides the energy density, equation-of-state parameter, and skewness parameters for the KHDE. Sections 6 and 7 give the stability analysis and the energy conditions, respectively. Section 8 illustrates the evolution graphically. The statefinder, Om, ω–ω' and Generalized Second Law diagnostics are added to the study in Section 9, along with three-dimensional parameter dependency visualizations. Section 10 concludes.

2 Metric and Field Equations

The anisotropic Bianchi type-V space-time is

$$ds^2 = -dt^2 + P^2dx^2 + e^{2x}(Q^2dy^2 + R^2dz^2) \tag{1}$$

where the metric potentials P, Q and R are functions of cosmic time *t*.

The field equations of Barber's second self-creation theory of gravitation are

$$G_j^i = R_j^i - \frac{1}{2}\delta_j^i R = -\frac{8\pi}{\phi}\left(T_j^i + \bar{T}_j^i\right) \tag{2}$$

where G_j^i is the Einstein tensor and T_j^i and $\bar{T}_j^i$ are the energy–momentum tensors of dark matter and KHDE, respectively.

The scalar field ϕ satisfies

$$\phi_{;k}^{,k} = \frac{8\pi}{3}\mu T \tag{3}$$

where T is the trace of the total energy–momentum tensor and μ is a coupling constant to be determined from experiment. The measurement of the deflection of light restricts the coupling constant to $|\mu| \leq 0.1$.

The energy–momentum tensor of pressureless dark matter (DM) is

$$T_j^i = \mathrm{diag}[0,0,0,-\rho_m] \tag{4}$$

and that of the anisotropic KHDE fluid is

$$\bar{T}_j^i = \mathrm{diag}[\omega_{de}\rho_{de}, (\omega_{de}+\delta)\rho_{de}, (\omega_{de}+\gamma)\rho_{de}, -\rho_{de}] \tag{5}$$

where ω_{de} is the equation-of-state (EoS) parameter. The parameters δ and γ measure the deviation of the pressure from ω_{de} along the y- and z-axes, respectively (skewness parameters).

For the metric (1), Eqs. (4) and (5) turn the field equations (2) into

$$-\frac{1}{P^2}+\frac{\ddot{Q}}{Q}+\frac{\ddot{R}}{R}+\frac{\dot{Q}\dot{R}}{QR} = -8\pi\phi^{-1}\omega_{de}\rho_{de} \tag{6}$$

$$-\frac{1}{P^2}+\frac{\ddot{P}}{P}+\frac{\dot{P}\dot{R}}{PR}+\frac{\ddot{R}}{R} = -8\pi\phi^{-1}(\omega_{de}+\delta)\rho_{de} \tag{7}$$

$$-\frac{1}{P^2}+\frac{\ddot{P}}{P}+\frac{\dot{P}\dot{Q}}{PQ}+\frac{\ddot{Q}}{Q} = -8\pi\phi^{-1}(\omega_{de}+\gamma)\rho_{de} \tag{8}$$

$$-\frac{3}{P^2}+\frac{\dot{P}\dot{Q}}{PQ}+\frac{\dot{P}\dot{R}}{PR}+\frac{\dot{Q}\dot{R}}{QR} = 8\pi\phi^{-1}(\rho_{de}+\rho_m) \tag{9}$$

$$\frac{2\dot{P}}{P}-\frac{\dot{Q}}{Q}-\frac{\dot{R}}{R} = 0 \tag{10}$$

and Eq. (3) gives

$$\ddot{\phi}+\dot{\phi}\left(\frac{\dot{P}}{P}+\frac{\dot{Q}}{Q}+\frac{\dot{R}}{R}\right) = \frac{8\pi\mu}{3}[-\rho_m+(3\omega_{de}+\delta+\gamma-1)\rho_{de}] \tag{11}$$

where an overdot denotes differentiation with respect to *t*.

3 Solutions of the Field Equations

Equations (6)–(11), together with the KHDE density (28) of Section 5, form seven equations in the nine unknowns $P, Q, R, \phi, \omega_{de}, \delta, \gamma, \rho_{de}, \rho_m$. Two additional physical conditions are therefore needed.

3.1 A constraint on the skewness parameters. Integrating Eq. (10), with the integration constant set to unity, gives

$$P^2 = QR \tag{12}$$

Write $H_x = \dot{P}/P$, $H_y = \dot{Q}/Q$ and $H_z = \dot{R}/R$ for the directional Hubble parameters and $V = PQR$ for the spatial volume. Subtracting Eq. (7) and Eq. (8) from Eq. (6) gives

$$\frac{1}{V}\frac{d}{dt}\left[V\left(H_y-H_x\right)\right] = 8\pi\phi^{-1}\delta\rho_{de}, \qquad \frac{1}{V}\frac{d}{dt}[V(H_z-H_x)] = 8\pi\phi^{-1}\gamma\rho_{de} \tag{13}$$

By Eq. (12), $H_x = \frac{1}{2}\left(H_y+H_z\right)$, so $H_y-H_x = -(H_z-H_x)$ and Eq. (13) yields

$$\delta = -\gamma \tag{14}$$

This identity holds for every solution of the Bianchi type-V field equations. In particular, if any two principal pressures of the dark-energy fluid are equal, then δ = γ = 0 and the fluid is isotropic. This is why both skewness parameters are retained in Eq. (5). By Eq. (14), the mean pressure of the KHDE fluid is $\bar{p}_{de} = \omega_{de}\rho_{de}$, so the trace in Eq. (11) is $T = -\rho_m + (3\omega_{de}-1)\rho_{de}$.

3.2 Closing conditions. (i) Following Collins et al. [24], we assume that the shear is proportional to the expansion through the relation

$$Q = R^k \tag{15}$$

where $k \neq 1$ is a constant (k = 1 recovers isotropy). Defining the average scale factor $a = V^{1/3}$, Eqs. (12) and (15) give

$$P = a, \qquad Q = a^{\frac{2k}{k+1}}, \qquad R = a^{\frac{2}{k+1}} \tag{16}$$

(ii) Assumed expansion laws are a standard way to close anisotropic cosmological models in scalar–tensor theories [26,27]. We adopt the hybrid expansion law (HEL) [25]

$$a(t) = a_0 t^{\alpha} e^{\beta t}, \qquad \alpha > 0,\ \beta > 0 \tag{17}$$

where $a_0 > 0$ is a constant. The HEL combines a power law, which dominates at early times, with an exponential law, which dominates at late times, and so allows a transition from deceleration to acceleration. The metric potentials are then

$$P = a_0 t^{\alpha} e^{\beta t}, \qquad Q = \left(a_0 t^{\alpha} e^{\beta t}\right)^{\frac{2k}{k+1}}, \qquad R = \left(a_0 t^{\alpha} e^{\beta t}\right)^{\frac{2}{k+1}} \tag{18}$$

and the Bianchi type-V KHDE model in self-creation theory becomes

$$ds^2 = -dt^2 + a_0^2 t^{2\alpha} e^{2\beta t} dx^2 + e^{2x}\left[\left(a_0 t^{\alpha} e^{\beta t}\right)^{\frac{4k}{k+1}} dy^2 + \left(a_0 t^{\alpha} e^{\beta t}\right)^{\frac{4}{k+1}} dz^2\right] \tag{19}$$

3.3 The scalar field. Equations (6)–(9) express the trace of the total energy–momentum tensor through the geometry as $T = -\phi\mathcal{R}/8\pi$, where $\mathcal{R}$ is the Ricci scalar of the metric (19). Equation (11) therefore becomes a linear equation for ϕ:

$$\ddot{\phi} + 3H\dot{\phi} + \frac{\mu}{3}\mathcal{R}\phi = 0, \qquad \mathcal{R} = 6\left(\dot{H} + 2H^2\right) + 2\sigma^2 - \frac{6}{a^2} \tag{20}$$

where H and σ^2 are the Hubble parameter and shear scalar given in Section 4. The vanishing-trace condition used in [23] would require $\mathcal{R} \equiv 0$. For the metric (19), $\mathcal{R}$ is strictly positive (its minimum on the interval considered is 0.23 for the representative parameters of Section 8), so this condition cannot hold, and we do not impose it. For $\mu \to 0$, Eq. (20) has the exact solution $\phi = \phi_1 + \phi_2 \int V^{-1} dt$. For $\mu \neq 0$ we integrate Eq. (20) numerically from $t_i = 0.5$ with $\phi(t_i) = 1$ and $\dot{\phi}(t_i) = 0$.

4 Physical and Kinematical Parameters of the Model

The spatial volume and the average scale factor are

$$V = a^3 = a_0^3 t^{3\alpha} e^{3\beta t} \tag{21}$$

The mean Hubble parameter $H = \frac{1}{3}\left(H_x + H_y + H_z\right)$ and the expansion scalar $\theta = 3H$ are

$$H = \frac{\alpha}{t} + \beta, \qquad \theta = 3\left(\frac{\alpha}{t} + \beta\right) \tag{22}$$

with directional Hubble parameters $H_x = H$, $H_y = \frac{2k}{k+1}H$ and $H_z = \frac{2}{k+1}H$.

Deceleration parameter. The deceleration parameter $q = -a\ddot{a}/\dot{a}^2$ tells whether the expansion is slowing down (q > 0) or speeding up (q < 0). From Eq. (17), $\dot{H} = -\alpha/t^2$, and therefore

$$q = -\frac{a\ddot{a}}{\dot{a}^2} = -1 - \frac{\dot{H}}{H^2} = -1 + \frac{\alpha/t^2}{\left(\frac{\alpha}{t}+\beta\right)^2} = -1 + \frac{\alpha}{(\alpha+\beta t)^2} \tag{23}$$

At early times, $q \to 1/\alpha - 1$, which is positive for $0 < \alpha < 1$. As $t \to \infty$, $q \to -1$, the de Sitter limit. Since $dq/dt = -2\alpha\beta/(\alpha+\beta t)^3 < 0$, q decreases monotonically. It vanishes when $(\alpha+\beta t)^2 = \alpha$, that is at the transition time

$$t_{tr} = \frac{\sqrt{\alpha}-\alpha}{\beta} \tag{24}$$

which is positive only for $0 < \alpha < 1$. The model therefore describes a single, smooth transition from an early decelerating phase to the present accelerating phase. For the representative values α = 0.5 and β = 0.1, $q(t \to 0) = 1$ and $t_{tr} = 2.07$. Table 1 lists q at selected epochs.

Table 1 *Deceleration parameter q from Eq. (23) at selected epochs (α = 0.5, β = 0.1)*

Cosmic time t	Deceleration parameter q	Phase
0.5	0.653	decelerating
1	0.389	decelerating
2.07 (t_{tr})	0	transition
3	−0.219	accelerating
5	−0.500	accelerating
5.54 (t_0)	−0.550	accelerating
8	−0.704	accelerating
10	−0.778	accelerating

The present epoch t_0 is defined in Section 8 by $q(t_0) = -0.55$. In terms of the redshift $1 + z = a(t_0)/a(t)$, q(z) follows parametrically from Eqs. (17) and (23). The corresponding transition redshift $z_{tr} = a(t_0)/a(t_{tr}) - 1$ is 1.10, 1.31 and 1.58 for α = 0.45, 0.5 and 0.55. These values are higher than the observational estimates $z_{tr} \approx 0.5$–0.8, which again shows that the illustrative parameters still need an observational fit. The behaviour of q is shown in Fig. 3.

Here the average anisotropy parameter (A_h) and the shear scalar (σ^2) are

$$A_h = \frac{1}{3}\sum_i \left(\frac{H_i - H}{H}\right)^2 = \frac{2(k-1)^2}{3(k+1)^2}, \qquad \sigma^2 = \frac{(k-1)^2}{(k+1)^2}\left(\frac{\alpha}{t}+\beta\right)^2 \tag{25}$$

Both A_h and $\sigma/\theta = |k-1|/\big(3(k+1)\big)$ are constant. The shear scalar decreases with time and tends to $\beta^2(k-1)^2/(k+1)^2$. This is a direct consequence of the Collins relation (15): the anisotropy does not die away relative to the expansion, and its level is set by $|k-1|$. For k = 0.8, $A_h = 0.0082$ and $\sigma/\theta = 0.037$, so the model is close to isotropic, and observations of the present near-isotropic universe require k close to unity.

5 Kaniadakis Holographic Dark Energy: Density, Equation of State and Skewness Parameters

In KHDE, the total vacuum energy inside a region of size $\mathcal{L}$ must not exceed the energy of a black hole of the same size, whose entropy is the Kaniadakis entropy $S_\mathcal{K} = \mathcal{K}^{-1}\sinh(\mathcal{K}A/4)$. This gives

$$\rho_{de} \propto \frac{S_\mathcal{K}}{\mathcal{L}^4} \tag{26}$$

Taking the Hubble horizon as the IR cutoff ($\mathcal{L} = 1/H$, $A = 4\pi/H^2$) gives

$$\rho_{de} = \frac{3c^2H^4}{\mathcal{K}}\sinh\left(\frac{\pi\mathcal{K}}{H^2}\right) \tag{27}$$

where c^2 is a dimensionless constant and $\mathcal{K}$ is the real Kaniadakis parameter. Since $\mathcal{K}^{-1}\sinh(\pi\mathcal{K}/H^2) \to \pi/H^2$ as $\mathcal{K} \to 0$, the standard HDE density $\rho_{de} \to 3\pi c^2H^2$ is recovered in that limit. Using Eq. (22), the KHDE energy density is

$$\rho_{de} = \frac{3c^2}{\mathcal{K}}\left(\frac{\alpha}{t}+\beta\right)^4 \sinh\left(\frac{\pi\mathcal{K}}{\left(\frac{\alpha}{t}+\beta\right)^2}\right) \tag{28}$$

As a function of H, ρ_{de} increases with H, so it decreases with time, as long as $\tanh x > x/2$ with $x = \pi\mathcal{K}/H^2$, that is for $x < 1.915$. With $H \geq 0.15$ on the interval considered, ρ_{de} decreases monotonically for $\mathcal{K} < 0.0137$.

From Eqs. (9), (16) and (25), the total energy density is

$$\rho_{de} + \rho_m = \frac{\phi}{8\pi}\left[3H^2 - \sigma^2 - \frac{3}{a^2}\right] \tag{29}$$

so the dark-matter energy density is

$$\rho_m = \frac{\phi}{8\pi}\left[\frac{2(k^2+4k+1)}{(k+1)^2}\left(\frac{\alpha}{t}+\beta\right)^2 - \frac{3}{a_0^2 t^{2\alpha} e^{2\beta t}}\right] - \frac{3c^2}{\mathcal{K}}\left(\frac{\alpha}{t}+\beta\right)^4 \sinh\left(\frac{\pi\mathcal{K}}{\left(\frac{\alpha}{t}+\beta\right)^2}\right) \tag{30}$$

The term $-3/a^2$ reflects the open (negative) spatial curvature of the Bianchi type-V geometry. It decays exponentially under the HEL, so it does not drive the total density negative, as it would for a power-law volume $V \propto t$.

From Eq. (6), the EoS parameter of KHDE is

$$\omega_{de} = \frac{\phi}{8\pi\rho_{de}}\left[\frac{1}{a^2} - 2\dot{H} - 3H^2 - \sigma^2\right] = \frac{\phi}{8\pi\rho_{de}}\left[\frac{1}{a_0^2 t^{2\alpha} e^{2\beta t}} + \frac{2\alpha}{t^2} - \frac{4(k^2+k+1)}{(k+1)^2}\left(\frac{\alpha}{t}+\beta\right)^2\right] \tag{31}$$

with ρ_{de} given by Eq. (28) and ϕ by Eq. (20).

From Eqs. (13), (14), (16) and (22), the skewness parameters are

$$\gamma = -\delta = \frac{\phi}{8\pi\rho_{de}}\frac{1-k}{1+k}\left(\dot{H} + 3H^2\right) = \frac{\phi}{8\pi\rho_{de}}\frac{1-k}{1+k}\left[3\left(\frac{\alpha}{t}+\beta\right)^2 - \frac{\alpha}{t^2}\right] \tag{32}$$

They vanish for k = 1, change sign with $1-k$, and are non-zero because $V(H_z - H_x) \propto a^3 H$ is not constant under the HEL.

6 Stability Analysis

Since δ + γ = 0, the mean pressure of the KHDE fluid is

$$\bar{p}_{de} = \omega_{de}\rho_{de} \tag{33}$$

and the squared sound speed is

$$v_s^2 = \frac{\dot{\bar{p}}_{de}}{\dot{\rho}_{de}} = \omega_{de} + \rho_{de}\frac{\dot{\omega}_{de}}{\dot{\rho}_{de}} \tag{34}$$

A positive v_s^2 indicates a classically stable configuration, a negative value signals instability against small perturbations, and causality further requires $v_s^2 \leq 1$. Since $\dot{\rho}_{de} < 0$ throughout for the parameters used, Eq. (34) is regular. Its evolution is shown in Fig. 9.

7 Energy Conditions

For the KHDE fluid with energy density ρ_{de} and mean pressure $\bar{p}_{de}$, the standard energy conditions are:

(i) Null energy condition (NEC): $\rho_{de} + \bar{p}_{de} \geq 0$

(ii) Weak energy condition (WEC): $\rho_{de} \geq 0$ and $\rho_{de} + \bar{p}_{de} \geq 0$

(iii) Strong energy condition (SEC): $\rho_{de} + 3\bar{p}_{de} \geq 0$ and $\rho_{de} + \bar{p}_{de} \geq 0$

(iv) Dominant energy condition (DEC): $\rho_{de} \geq |\bar{p}_{de}|$

Because $\rho_{de} > 0$, these reduce to conditions on ω_{de}: NEC requires $\omega_{de} \geq -1$, SEC requires $\omega_{de} \geq -1/3$, and DEC requires $-1 \leq \omega_{de} \leq 1$. They are displayed in Fig. 10 and discussed in Section 8.

8 Graphical Discussion

For the figures, the free constants take the representative values $\alpha = 0.5$, $\beta = 0.1$, $a_0 = 3$, $k = 0.8$, $c^2 = 0.006$, $\mathcal{K} = 0.012$ and $\mu = 0.05$, with $t \in [0.5, 10]$, and $\phi(0.5) = 1$, $\dot{\phi}(0.5) = 0$. These values are illustrative, not observationally fitted. They were chosen so that (i) $\rho_m > 0$ over the whole interval, (ii) ρ_{de} decreases monotonically ($\mathcal{K} < 0.0137$, Section 5), and (iii) the model passes from deceleration to acceleration. We call "present" the epoch t_0 at which $q(t_0) = -0.55$, which gives $t_0 = 5.54$. At t_0 the model has $H_0 = 0.190$, $\Omega_{de} \equiv \rho_{de}/(\rho_{de} + \rho_m) = 0.72$, $\omega_{de} = -1.10$, $\gamma = 0.16$ and $(r, s) = (0.504, 0.158)$. To test robustness, each figure shows three values of the parameter that most directly shapes the plotted quantity (solid, dashed and dash-dotted curves), with the other parameters held at their representative values.

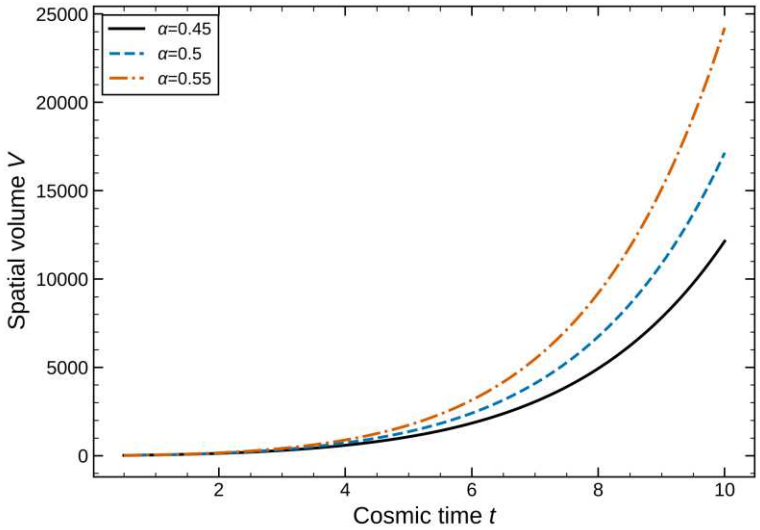


Fig. 1 Spatial volume V versus cosmic time t for three values of α. The volume increases monotonically, and the late-time growth is exponential, as required by the hybrid expansion law

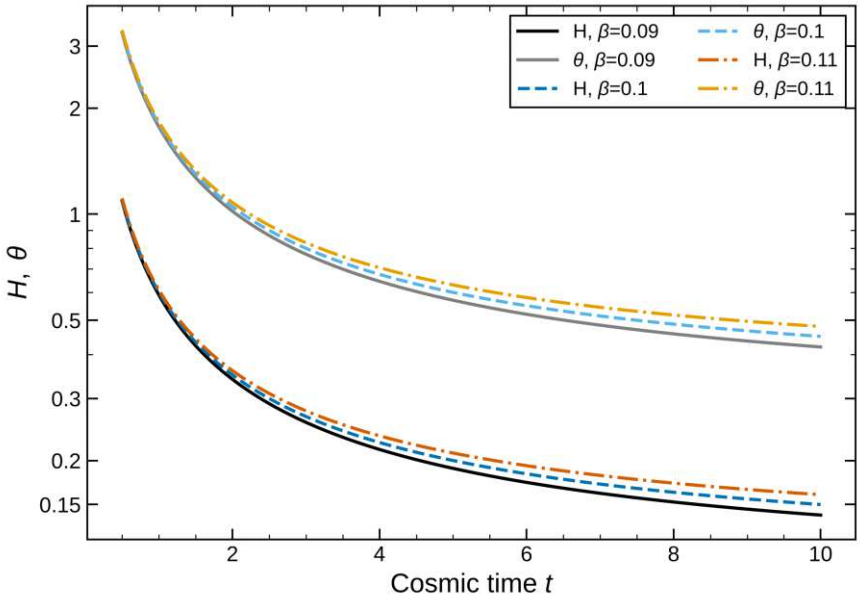


Fig. 2 Hubble parameter H and expansion scalar θ = 3H versus cosmic time t for three values of β (logarithmic scale). Both decrease with time and approach the constants β and 3β at late times

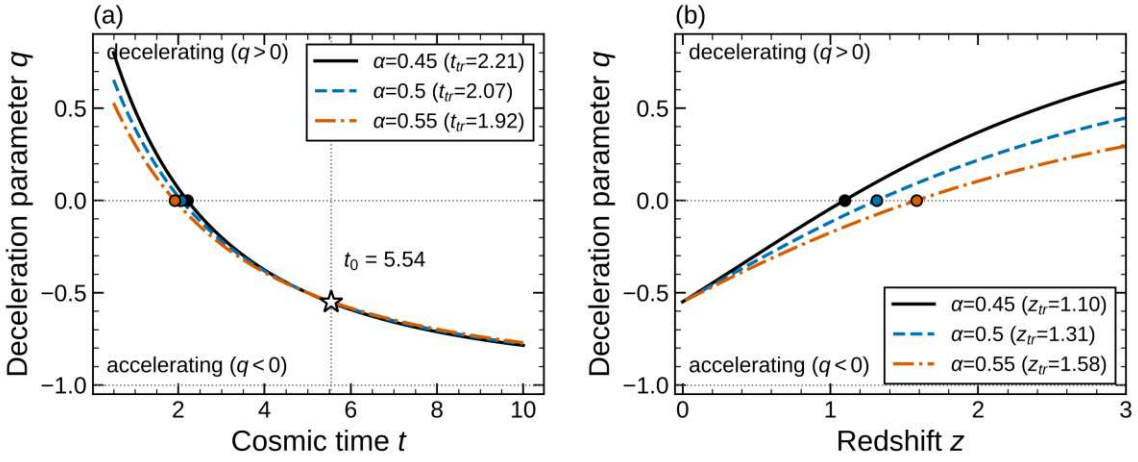


Fig. 3 Deceleration parameter q from Eq. (23) for three values of α (β = 0.1): (a) versus cosmic time t and (b) versus redshift z, with z = 0 at the present epoch q = −0.55. The filled circles mark the transition from deceleration (q > 0) to acceleration (q < 0), at t_{tr} = 2.21, 2.07 and 1.92, or equivalently z_{tr} = 1.10, 1.31 and 1.58, for α = 0.45, 0.5 and 0.55. The star marks the present epoch t_0 = 5.54. q decreases monotonically towards the de Sitter value −1

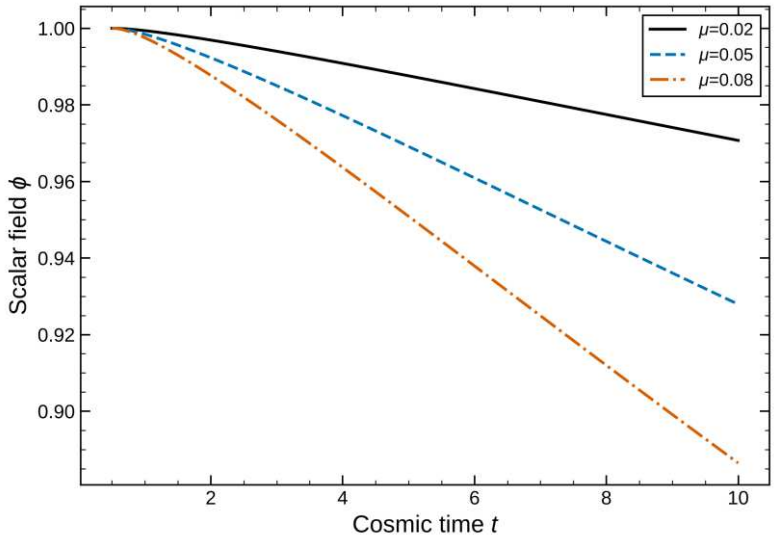


Fig. 4 Scalar field φ obtained by integrating Eq. (20) for three values of the coupling constant μ. φ decreases slowly, by 3%, 7% and 11% over the interval for μ = 0.02, 0.05 and 0.08, so the effective gravitational coupling $8\pi/\varphi$ grows slightly

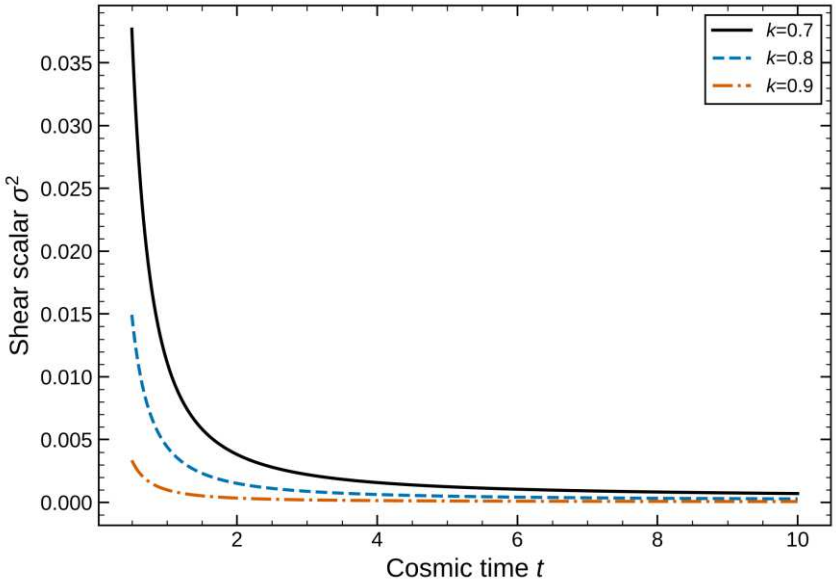


Fig. 5 Shear scalar σ^2 versus cosmic time t for three values of the Collins exponent k. σ^2 decreases and tends to $\beta^2(k-1)^2/(k+1)^2$. A larger $|k-1|$ gives larger anisotropy, while σ/θ stays constant

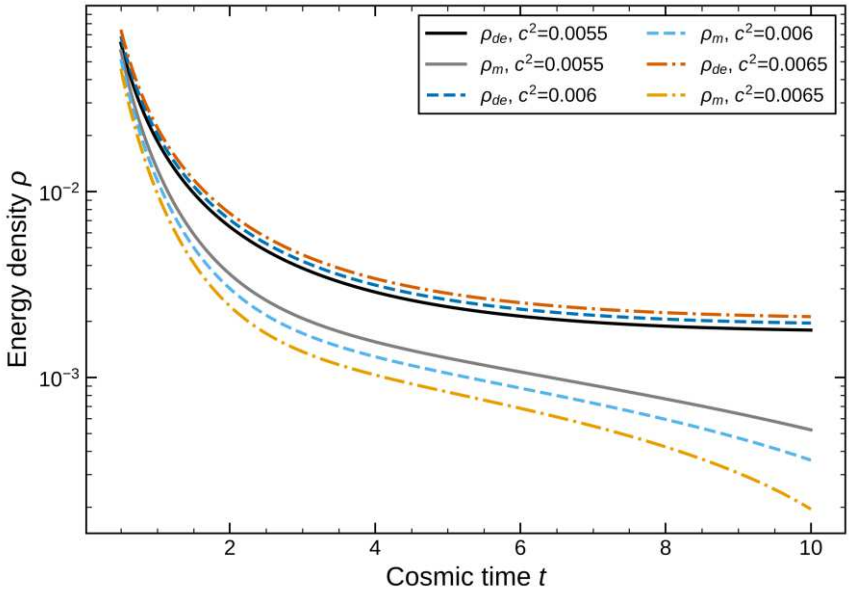


Fig. 6 Energy densities of KHDE (ρ_{de}) and dark matter (ρ_m) versus cosmic time t for three values of c^2 (logarithmic scale). Both remain positive and decrease. The KHDE density decays more slowly and dominates at late times; Ω_{de} grows from 0.57 at t = 0.5 to 0.85 at t = 10 for $c^2 = 0.006$. A larger c^2 raises ρ_{de} and lowers ρ_m

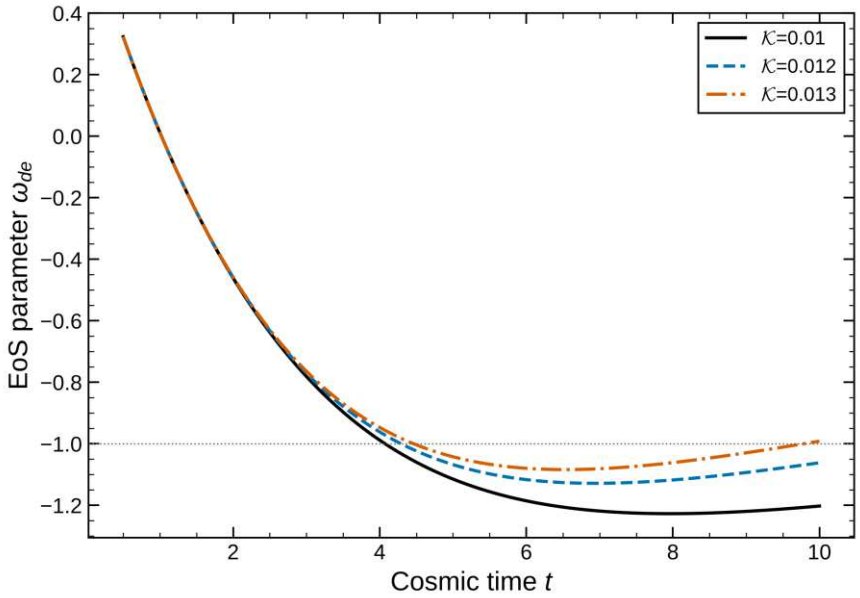


Fig. 7 EoS parameter ω_{de} of KHDE versus cosmic time t for three values of the Kaniadakis parameter $\mathcal{K}$. ω_{de} starts from a matter-like positive value (0.32), enters the quintessence region ($-1 < \omega_{de} < -1/3$) at $t \approx 1.7$, and crosses the phantom divide at $t \approx 4.1$–4.5. It reaches a minimum (−1.23, −1.13 and −1.08 for $\mathcal{K}$ = 0.010, 0.012 and 0.013) and then turns back towards −1. A larger $\mathcal{K}$ gives a milder phantom phase

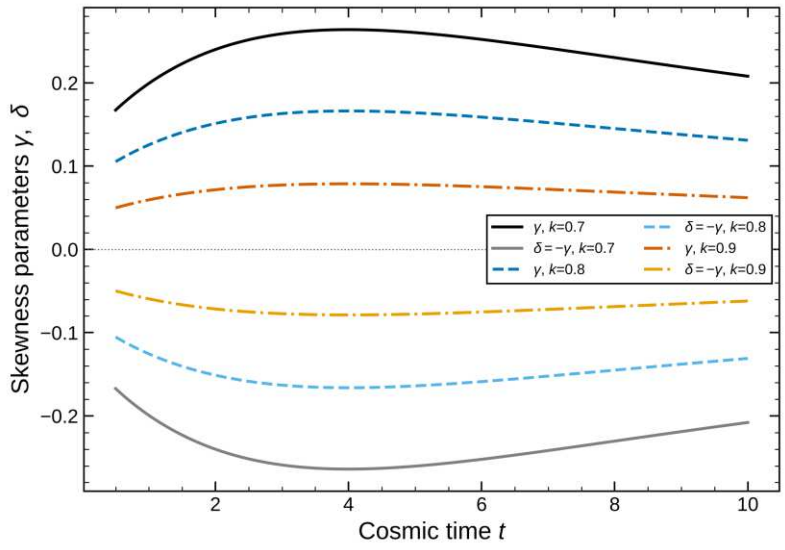


Fig. 8 Skewness parameters γ and δ = −γ versus cosmic time t for three values of k. The parameters are of order 0.1, vary slowly, vanish as k → 1, and have magnitudes that grow with |1−k|

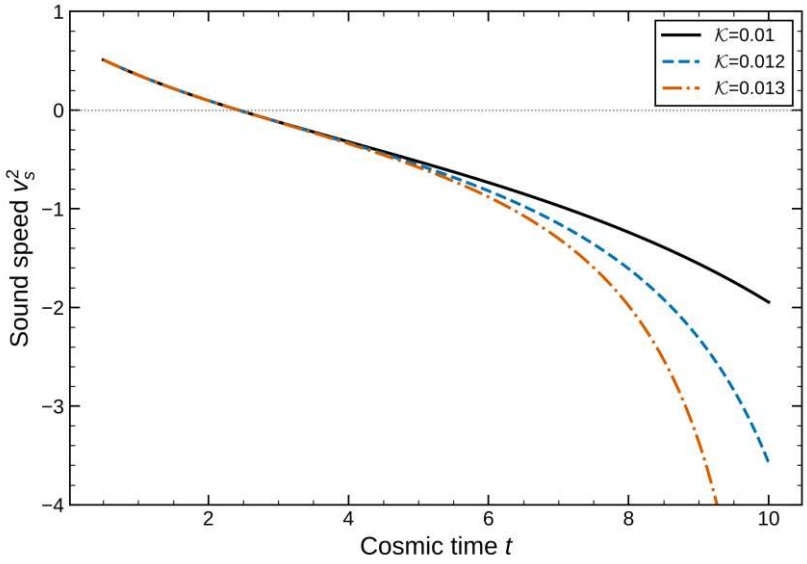


Fig. 9 Squared sound speed v_s^2 versus cosmic time t for three values of $\mathcal{K}$. v_s^2 is positive (stable) in the early decelerating era and becomes negative at t ≈ 2.43, so the KHDE fluid is classically unstable at late times. This instability is common to holographic dark-energy models with a Hubble cutoff, and a larger $\mathcal{K}$ deepens it

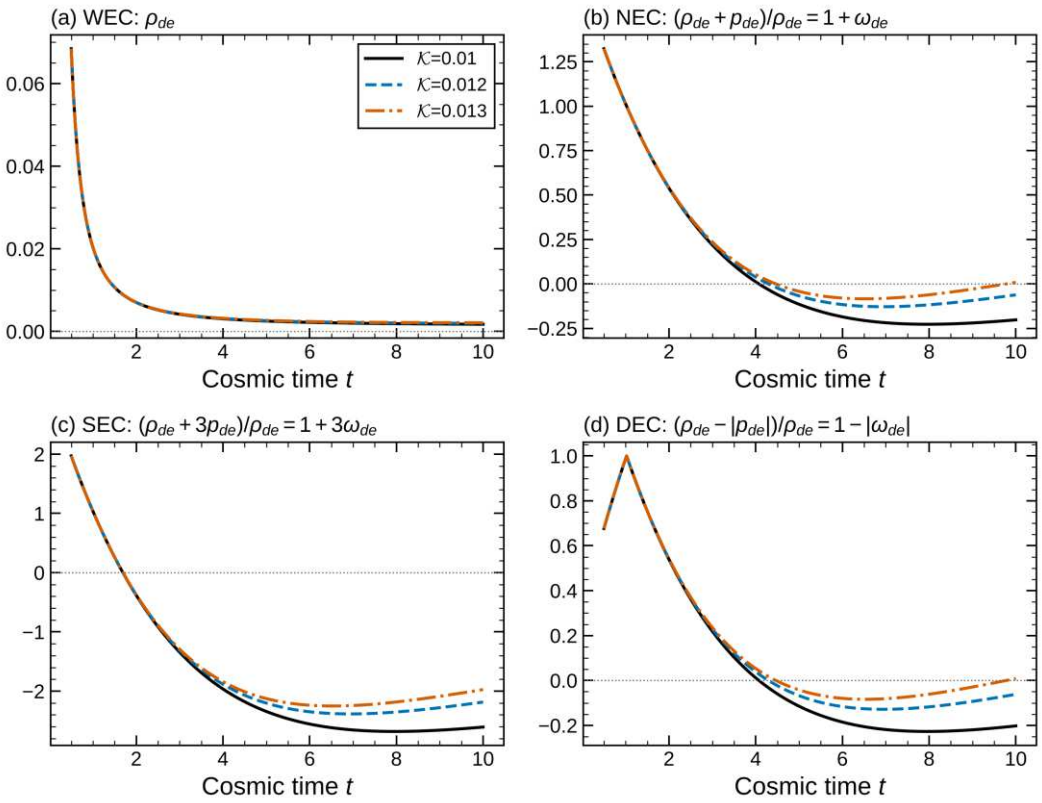


Fig. 10 Energy conditions for three values of $\mathcal{K}$: ρ_{de} (WEC), $1 + \omega_{de}$ (NEC), $1 + 3\omega_{de}$ (SEC) and $1 - |\omega_{de}|$ (DEC), each normalized by $\rho_{de} > 0$. The SEC is violated after $t \approx 1.7$, as required for dark energy that drives acceleration. The NEC, and with it the WEC and DEC, hold until the phantom crossing at $t \approx 4.3$ and are violated in the phantom phase

9 Additional Validation and Diagnostic Tools

This section applies a set of complementary diagnostics that compare the model with ΛCDM and with other dark-energy models. Each diagnostic is built from the average scale factor (17), the scalar field (20) and the KHDE quantities of Section 5, so no further field-equation solutions are required.

9.1 Statefinder Diagnostic {r, s}

Sahni et al. [28] introduced the statefinder pair to discriminate between dark-energy models with the same present values of H and q:

$$r = \frac{\dddot{a}}{aH^3} = 1 - \frac{3\alpha}{t^2H^2} + \frac{2\alpha}{t^3H^3}, \qquad s = \frac{r-1}{3\left(q-\frac{1}{2}\right)} \tag{35}$$

with H given by Eq. (22). Rather than a fixed point, {r, s} traces a trajectory in this model (Fig. 11). During the decelerating era the trajectory passes through the ΛCDM point (r, s) = (1, 0) at $t = (2/3 - \alpha)/\beta \approx 1.67$. It then enters the region $r < 1$, $s > 0$, a signature of quintessence-like expansion, with (r, s) = (0.504, 0.158) at t_0. As $t \to \infty$, $H \to \beta$ and the trajectory returns to the ΛCDM point. The parameter s is undefined where $q = 1/2$ ($t \approx 0.77$ for $\alpha = 0.5$), so that point is excluded from the figure.

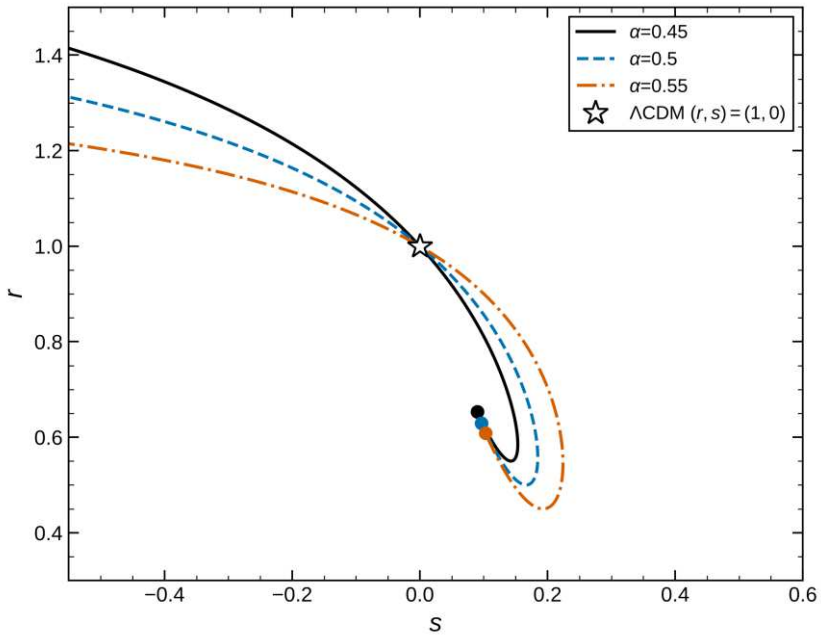


Fig. 11 Statefinder {r, s} trajectory for three values of α. The filled dots mark t = 10 and the star marks the ΛCDM point (r, s) = (1, 0). The trajectories approach ΛCDM at late times

9.2 Om(t) Diagnostic

The Om diagnostic of Sahni, Shafieloo and Starobinsky [29] depends only on H. Written in cosmic time, it is

$$Om(t) = \frac{\left(\frac{H(t)}{H_0}\right)^2 - 1}{\left(\frac{a(t_0)}{a(t)}\right)^3 - 1} \tag{36}$$

where $H_0 = H(t_0)$ and $1 + z = a(t_0)/a(t)$. Om is constant for ΛCDM. In this model it varies from about 0.18 to 0.42 over the interval (Fig. 12). For t $\gtrsim$ 1.1, Om increases with t, which means it decreases with redshift, the signature of quintessence-like behaviour of the effective total fluid. This agrees with the statefinder result, because the effective total EoS $\omega_{eff} = (2q - 1)/3$ stays above −1 whenever $\dot{H} < 0$. The dark-energy component alone can still cross −1, because dark matter carries part of the total density.

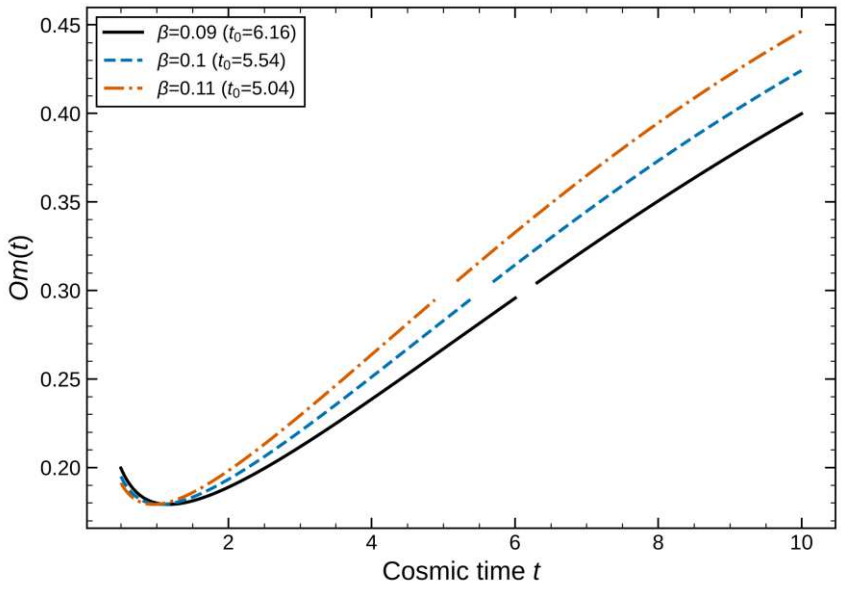


Fig. 12 Om(t) diagnostic for three values of β, each relative to its own present epoch t_0 ($q(t_0) = -0.55$). The point $t = t_0$, where Eq. (36) is 0/0, is omitted. Om varies clearly with time, confirming the departure from ΛCDM

9.3 ω–ω′ Phase Plane

In the (ω, ω′) plane of Caldwell and Linder [30], with $\omega' = d\omega_{de}/d\ln a = \dot{\omega}_{de}/H$, the region $\omega' < 0$, $\omega < 0$ corresponds to "freezing" and the region $\omega' > 0$, $\omega < 0$ to "thawing" evolution. In the present model (Fig. 13), $\omega' < 0$ for most of the evolution, so the KHDE freezes from $\omega_{de} \approx 0.32$ into the phantom region. Near the minimum of ω_{de} ($t \approx 6.9$ for $\mathcal{K} = 0.012$), ω' changes sign and the trajectory turns back towards $\omega = -1$ with $\omega' > 0$.

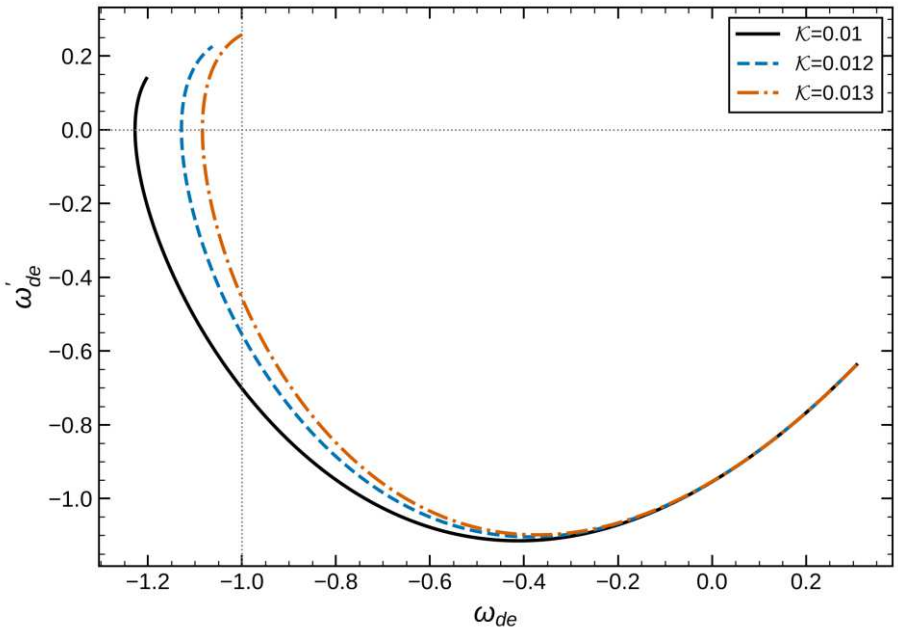


Fig. 13 ω–ω′ phase-plane trajectory of KHDE for three values of $\mathcal{K}$. The dotted lines mark $\omega' = 0$ and the phantom divide $\omega = -1$

9.4 Thermodynamic Validation: Generalized Second Law (GSL)

We test the GSL [31] at the apparent horizon of the average (open, FRW-like) geometry, following the approach of [32,33]. The apparent horizon radius, its temperature and its entropy are

$$R_A = \frac{1}{\sqrt{H^2 - a^{-2}}}, \qquad T_A = \frac{1}{2\pi R_A}, \qquad S_h = \pi R_A^2 \phi \tag{37}$$

where the horizon entropy uses the effective coupling $G_{eff} = \phi^{-1}$ of Eq. (2). $H^2 > a^{-2}$ holds throughout, with a minimum of 0.021. Self-creation theory does not conserve energy in the usual way, so the entropy of the fluid inside the horizon is obtained directly from the Gibbs relation, without assuming a continuity equation:

$$T_A \dot{S}_{in} = V_h \dot{\rho}_{tot} + (\rho_{tot} + \bar{p}) \dot{V}_h, \qquad V_h = \frac{4\pi}{3} R_A^3 \tag{38}$$

where $\rho_{tot} = \rho_{de} + \rho_m$ is given by Eq. (29) and $\bar{p} = \omega_{de} \rho_{de}$. The GSL requires $\dot{S}_{tot} = \dot{S}_h + \dot{S}_{in} \geq 0$. Fig. 14 shows that the GSL holds throughout t ∈ [0.5, 10] for μ = 0.02. For μ = 0.05 and μ = 0.08 it fails after t ≈ 7.4 and t ≈ 6.2, respectively. The violation comes from the decrease of φ (Fig. 4), which reduces the horizon entropy $\pi R_A^2 \phi$. The GSL therefore constrains the self-creation coupling: in this model, thermodynamic consistency up to t = 10 requires roughly μ ≲ 0.02. The test uses the average geometry, so it is approximate for an anisotropic metric, but the anisotropy is small (σ/θ = 0.037).

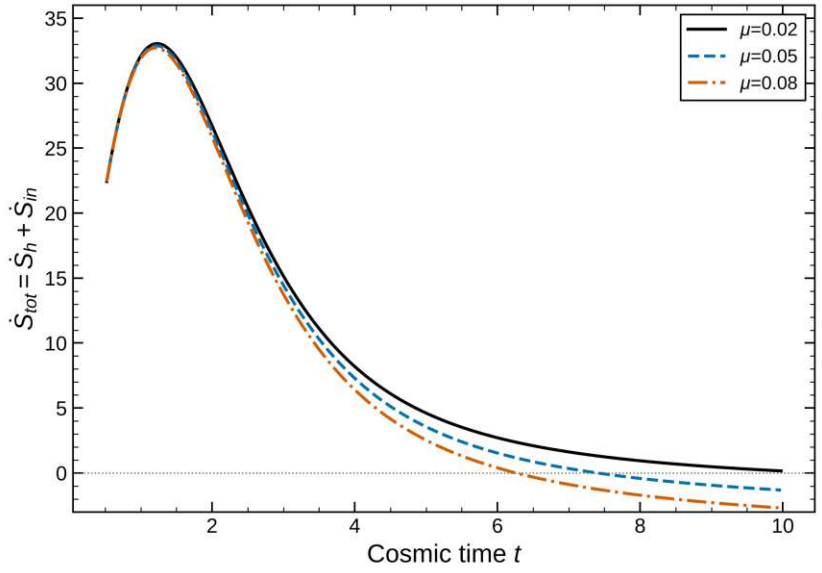


Fig. 14 Total entropy production rate $\dot{S}_{tot}$ at the apparent horizon for three values of μ. The GSL ($\dot{S}_{tot} \geq 0$) holds throughout for μ = 0.02 and fails at late times for larger couplings

9.5 Parameter Dependence: 3-D Surface Visualizations

The following surfaces sweep cosmic time and one free constant at a time, with the others held at their representative values.

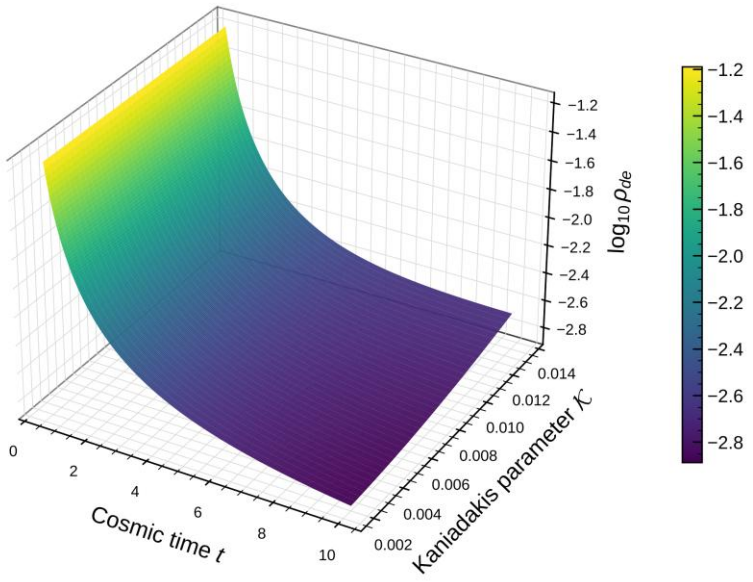


Fig. 15 3-D surface of $\log_{10}\rho_{de}(t, \mathcal{K})$ from Eq. (28) for $0.002 \leq \mathcal{K} \leq 0.0135$. ρ_{de} decreases monotonically in t throughout this range, and a larger $\mathcal{K}$ raises the late-time density

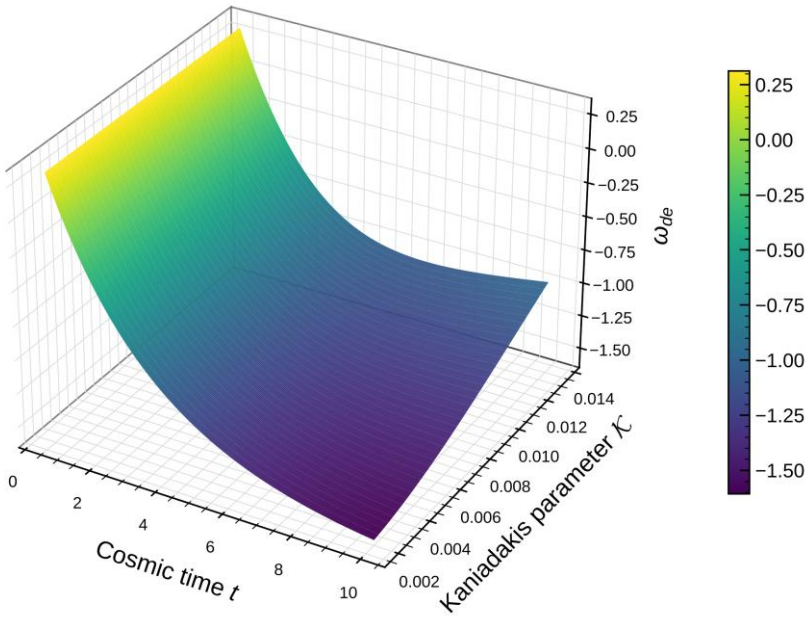


Fig. 16 3-D surface of the EoS parameter $\omega_{de}(t, \mathcal{K})$ from Eq. (31). Small $\mathcal{K}$ produces a deeper phantom phase (minimum below −1.5 for $\mathcal{K} = 0.002$). Increasing $\mathcal{K}$ raises Ω_{de} and keeps ω_{de} closer to −1

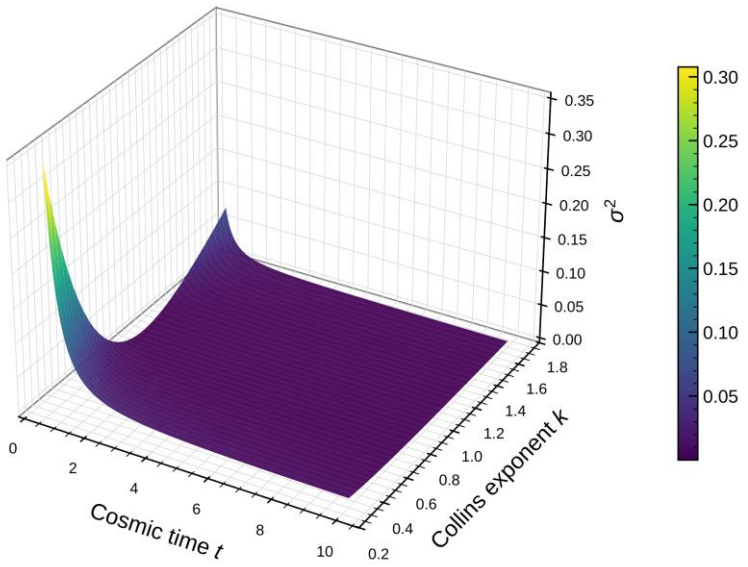


Fig. 17 3-D surface of the shear scalar $\sigma^2(t, k)$ from Eq. (25). σ^2 vanishes along $k = 1$ and grows with $|k-1|$

10 Conclusions

We have studied a spatially homogeneous and anisotropic Bianchi type-V universe containing dark matter and anisotropic Kaniadakis holographic dark energy in Barber's self-creation theory of gravity. The main findings are:

1. For the Bianchi type-V metric, the off-diagonal field equation forces the skewness parameters to satisfy $\delta = -\gamma$ (Eq. 14). A dark-energy fluid with two equal principal pressures is therefore necessarily isotropic, and an anisotropic fluid requires both δ and γ.

2. With the Collins relation and a hybrid expansion law, the field equations are solved exactly for the metric. The scalar-field equation reduces to the linear equation (20), driven by the Ricci scalar. A vanishing-trace condition is incompatible with this metric and is not used.

3. The spatial volume grows monotonically and exponentially at late times, while H and θ decrease towards β and 3β. The deceleration parameter, $q = -1 + \alpha/(\alpha + \beta t)^2$ (Eq. 23), decreases monotonically from $1/\alpha - 1$ and changes sign at $t_{tr} = (\sqrt{\alpha} - \alpha)/\beta \approx 2.07$ ($z_{tr} \approx 1.31$), so the model describes a transition from deceleration to the present accelerated expansion, and $q \to -1$ at late times.

4. The shear scalar decreases, but the anisotropy parameter $A_h = 2(k-1)^2/(3(k+1)^2)$ and the ratio σ/θ are constant. The model does not isotropize relative to the expansion; it stays close to isotropy only for k near unity ($A_h = 0.0082$ for $k = 0.8$).

5. The KHDE and dark-matter densities are positive and decreasing throughout, and KHDE dominates at late times ($\Omega_{de} = 0.72$ at the present epoch $t_0 = 5.54$).

6. The EoS parameter evolves from a matter-like value through the quintessence region and crosses the phantom divide at $t \approx 4.3$, giving quintom-like behaviour with $\omega_{de}(t_0) = -1.10$. The skewness parameters are finite ($|\gamma| \approx 0.1$–0.17 for $k = 0.8$) and vanish in the isotropic limit $k = 1$.

7. The squared sound speed is positive in the decelerating era and negative after $t \approx 2.43$, so the KHDE fluid is classically unstable at late times.

8. The SEC is violated after $t \approx 1.7$, consistent with accelerated expansion. The NEC, WEC and DEC hold until the phantom crossing and are violated in the phantom phase.

9. The statefinder pair follows a trajectory that passes through the ΛCDM point during deceleration, lies in the quintessence-like region $r < 1$, $s > 0$ at the present epoch, and approaches (1, 0) at late times. The Om(t) diagnostic varies with time, and the ω–ω' plane shows freezing evolution that turns back near the minimum of ω_{de}.

10. The Generalized Second Law at the apparent horizon holds throughout the interval for $\mu = 0.02$ but is violated at late times for $\mu = 0.05$ and 0.08, because φ decreases. Thermodynamic consistency therefore favours a weak self-creation coupling.

11. The 3-D surfaces show that the Kaniadakis parameter controls the depth of the phantom phase and the late-time dark-energy density, while the Collins exponent controls the anisotropy level.

12. The parameter values used here are illustrative and not the result of an observational fit. The next step is to constrain α, β, c^2, $\mathcal{K}$, k and μ with present data, for example the Planck constraints on the dark-energy equation of state [34] and model-independent estimates of the deceleration parameter [35], following the comparative approach used for related Kaniadakis holographic models [10].

Acknowledgements

Statements and Declarations

Funding The authors declare that no funds, grants, or other support were received during the preparation of this manuscript.

Competing interests The authors have no relevant financial or non-financial interests to disclose.

Author contributions M.P.V.V. BhaskaraRao: conceptualization, methodology, formal analysis, writing – original draft. Tenneti Ramprasad: formal analysis, validation, visualization, writing – review and editing. All authors read and approved the final manuscript.

Data availability This is a theoretical study and no external datasets were used. All quantities shown in the figures follow from the equations given in the text; the numerical data and the code used to integrate Eq. (20) and to produce the figures are available from the corresponding author on reasonable request.

Ethics approval and consent Not applicable.

References

1. Perlmutter, S., et al. (1999). Measurements of Ω and Λ from 42 high-redshift supernovae. *The Astrophysical Journal, 517*(2), 565–586. https://doi.org/10.1086/307221

2. Riess, A. G., et al. (1998). Observational evidence from supernovae for an accelerating universe and a cosmological constant. *The Astronomical Journal, 116*(3), 1009–1038. https://doi.org/10.1086/300499

3. Tegmark, M., et al. (2004). Cosmological parameters from SDSS and WMAP. *Physical Review D, 69*(10), 103501. https://doi.org/10.1103/PhysRevD.69.103501

4. Susskind, L. (1995). The world as a hologram. *Journal of Mathematical Physics, 36*(11), 6377–6396. https://doi.org/10.1063/1.531249

5. Bousso, R. (1999). A covariant entropy conjecture. *Journal of High Energy Physics, 1999*(07), 004. https://doi.org/10.1088/1126-6708/1999/07/004

6. Cohen, A. G., Kaplan, D. B., & Nelson, A. E. (1999). Effective field theory, black holes, and the cosmological constant. *Physical Review Letters, 82*(25), 4971–4974. https://doi.org/10.1103/PhysRevLett.82.4971

7. Tsallis, C., & Cirto, L. J. L. (2013). Black hole thermodynamical entropy. *The European Physical Journal C, 73*(10), 2487. https://doi.org/10.1140/epjc/s10052-013-2487-6

8. Moradpour, H., et al. (2018). Thermodynamic approach to holographic dark energy and the Rényi entropy. *The European Physical Journal C, 78*(10), 829. https://doi.org/10.1140/epjc/s10052-018-6309-8

9. Kaniadakis, G. (2001). Non-linear kinetics underlying generalized statistics. *Physica A: Statistical Mechanics and its Applications, 296*(3–4), 405–425. https://doi.org/10.1016/S0378-4371(01)00184-4

10. Moradpour, H., Ziaie, A. H., & Zangeneh, M. K. (2020). Generalized entropies and corresponding holographic dark energy models. *The European Physical Journal C, 80*(8), 732. https://doi.org/10.1140/epjc/s10052-020-8307-x

11. Jawad, A., & Sultan, A. M. (2021). Cosmic consequences of Kaniadakis and generalized Tsallis holographic dark energy models in the fractal universe. *Advances in High Energy Physics, 2021*, 5519028. https://doi.org/10.1155/2021/5519028

12. Drepanou, N., et al. (2022). Kaniadakis holographic dark energy and cosmology. *The European Physical Journal C, 82*, 449. https://doi.org/10.1140/epjc/s10052-022-10415-9

13. Vijaya Prasanthi, A., Suryanarayana, G., Aditya, Y., & Divya Prasanthi, U. Y. (2024). Cosmological dynamics of anisotropic Kaniadakis holographic dark energy model in Brans–Dicke gravity. *East European Journal of Physics*, (2), 10–20. https://doi.org/10.26565/2312-4334-2024-2-01

14. Aditya, Y., Tejeswararao, D., Divya Prasanthi, U. Y., & Ram Babu, D. (2025). Reconstruction of Kaniadakis holographic dark energy model in self creation theory of gravity. *East European Journal of Physics*, (1), 9–19. https://doi.org/10.26565/2312-4334-2025-1-01

15. Murali, K., Aditya, Y., & Kalesha Vali, S. (2024). Cosmographic analysis of anisotropic Kaniadakis holographic dark energy model. *Modern Physics Letters A, 39*(23–24), 2450106.

16. Ganeswara Rao, B., Mohanty, D. J., Aditya, Y., & Divya Prasanthi, U. Y. (2025). Bianchi type-VI_0 Kaniadakis holographic dark energy model in Brans–Dicke theory of gravity. *AIP Conference Proceedings, 3298*(1), 040021.

17. Vijaya Prasanthi, A., Suryanarayana, G., Aditya, Y., & Divya Prasanthi, U. Y. (2025). Cosmological evolution of Sharma–Mittal holographic dark energy in self creation theory of gravitation. *AIP Conference Proceedings, 3298*(1), 040034.

18. Rao, V. U. M., & Divya Prasanthi, U. Y. (2017). Bianchi type-V modified holographic Ricci dark energy model in self-creation theory of gravitation. *Canadian Journal of Physics, 95*(6), 554–558.

19. Ganeswara Rao, B., Mohanty, D. J., Aditya, Y., & Divya Prasanthi, U. Y. (2024). Cosmological evolution of Bianchi type-VI_0 Kaniadakis holographic dark energy model. *East European Journal of Physics*, (1), 43–54. https://doi.org/10.26565/2312-4334-2024-1-03

20. Reddy, D. R. K., et al. (2014). Bianchi type-II bulk viscous string cosmological model in self-creation theory of gravitation. *Astrophysics and Space Science, 351*, 385–389.

21. Barber, G. A. (1982). On two "self-creation" cosmologies. *General Relativity and Gravitation, 14*(2), 117–136. https://doi.org/10.1007/BF00756918

22. Bhaskara Rao, M. P. V. V., et al. (2026). Anisotropic Bianchi type-V generalized ghost pilgrim dark energy cosmological model in self-creation gravity. *Frontiers in Astronomy and Space Sciences, 13*, 1873551. https://doi.org/10.3389/fspas.2026.1873551

23. Reddy, D. R. K. (1987). Bianchi type-I universe filled with disordered radiation in self-creation cosmology. *Astrophysics and Space Science, 133*(2), 389–392. https://doi.org/10.1007/BF00642496

24. Collins, C. B., Glass, E. N., & Wilkinson, D. A. (1980). Exact spatially homogeneous cosmologies. *General Relativity and Gravitation, 12*(10), 805–823. https://doi.org/10.1007/BF00763057

25. Akarsu, Ö., Kumar, S., Myrzakulov, R., Sami, M., & Xu, L. (2014). Cosmology with hybrid expansion law: Scalar field reconstruction of cosmic history and observational constraints. *Journal of Cosmology and Astroparticle Physics, 2014*(01), 022. https://doi.org/10.1088/1475-7516/2014/01/022

26. Johri, V. B., & Sudharsan, R. (1989). BD-FRW cosmology with bulk viscosity. *Australian Journal of Physics, 42*(2), 215–222. https://doi.org/10.1071/PH890215

27. Johri, V. B., & Desikan, K. (1994). Cosmological models with constant deceleration parameter in Brans–Dicke theory. *General Relativity and Gravitation, 26*(12), 1217–1232. https://doi.org/10.1007/BF02106714

28. Sahni, V., Saini, T. D., Starobinsky, A. A., & Alam, U. (2003). Statefinder—A new geometrical diagnostic of dark energy. *JETP Letters, 77*, 201–206. https://doi.org/10.1134/1.1574831

29. Sahni, V., Shafieloo, A., & Starobinsky, A. A. (2008). Two new diagnostics of dark energy. *Physical Review D, 78*(10), 103502. https://doi.org/10.1103/PhysRevD.78.103502

30. Caldwell, R. R., & Linder, E. V. (2005). The limits of quintessence. *Physical Review Letters, 95*(14), 141301. https://doi.org/10.1103/PhysRevLett.95.141301

31. Izquierdo, G., & Pavón, D. (2006). Dark energy and the generalized second law. *Physics Letters B, 633*(4–5), 420–426.

32. Cai, R.-G., & Kim, S. P. (2005). First law of thermodynamics and Friedmann equations of Friedmann–Robertson–Walker universe. *Journal of High Energy Physics, 2005*(02), 050. https://doi.org/10.1088/1126-6708/2005/02/050

33. Akbar, M., & Cai, R.-G. (2007). Thermodynamic behavior of the Friedmann equation at the apparent horizon of the FRW universe. *Physical Review D, 75*(8), 084003. https://doi.org/10.1103/PhysRevD.75.084003

34. Planck Collaboration, Aghanim, N., et al. (2020). Planck 2018 results. VI. Cosmological parameters. *Astronomy & Astrophysics, 641*, A6. https://doi.org/10.1051/0004-6361/201833910

35. Capozziello, S., Ruchika, & Sen, A. A. (2019). Model-independent constraints on dark energy evolution from low-redshift observations. *Monthly Notices of the Royal Astronomical Society, 484*(4), 4484–4494.